Dominance of the two-nucleon mechanism in $^{16}O(\pi^+,pp)$ at 115 MeV

D. J. Mack,[a] P. G. Roos, H. Breuer, N. S. Chant, S. D. Hyman,[b] F. Khazaie,[c]
B. G. Ritchie,[d] and J. D. Silk[e]
University of Maryland, College Park, Maryland 20742

G. S. Kyle,[f] P. A. Amaudruz,[g] Th. S. Bauer,[h] C. H. Q. Ingram, D. Renker, R. A. Schumacher,[i] and
U. Sennhauser[j]
Paul Scherrer Institute, Villigen, Switzerland

W. J. Burger[k]
Massachusetts Institute of Technology, Bates Laboratory, Middleton, Massachusetts 01949
(Received 29 April 1991)

Singles $^{16}O(\pi^+,p)$ and coincidence $^{16}O(\pi^+,2p)^{14}N$ measurements have been made at $T_\pi = 115$ MeV over an extended range of the phase space of the two final-state protons. The coincidence measurements have a missing-mass resolution of 4 MeV. The direct two-nucleon absorption cross section extracted from the data is 58±8 mb. After corrections for final-state interactions, it was found that the two-nucleon $\pi^+ + np \rightarrow pp$ process accounts for about 76% of the total absorption cross section, and thus is the dominant absorption mechanism. Evidence for absorption on *s-p* pairs is seen as a broad bump near 32 MeV of excitation. At backward angles the inclusive $^{16}O(\pi^+,p)$ spectra show a distinct absorption peak, an important feature not previously observed. Comparisons of distorted wave impulse approximation calculations to both the coincidence data and inclusive data are presented.

PACS number(s): 25.80.Ls

I. INTRODUCTION

One of the most interesting questions in the field of pion absorption is that of the reaction mechanism; specifically, the number of nucleons which directly share the four-momentum of the incident pion. A dominant two-nucleon mechanism was hypothesized in an early study [1] of pion absorption. The existence of this mechanism was clearly demonstrated in the experiments of Favier *et al.* [2] with 76 MeV π^+ on a number of targets ranging from ^{4}He to Pb, and of Arthur *et al.* [3] with 70 MeV π^+ on ^{6}Li, ^{14}N, and ^{16}O. However, neither of these experiments attempted to quantify the two-nucleon absorption yield in comparison to the total absorption cross section. The dominance of the two-nucleon mechanism was questioned in light of the inclusive $(\pi^\pm,p)$ measurements of McKeown *et al.* [4] on nuclei ranging from ^{4}He to ^{181}Ta at energies of 100, 160, and 220 MeV. That group used extracted nucleon multiplicities and a rapidity analysis to suggest that the average number of nucleons participating in pion absorption was three to six depending upon target mass and incident energy. These results stimulated much of the later experimental and theoretical work of the last decade. A review of the status of pion absorption in nuclei is given in Ref. [5].

In light of past confusion we first clarify some of the terminology used herein. The assumption of a two-nucleon absorption mechanism does not preclude a prior π-N interaction in which a nucleon may be removed from the nucleus, referred to as initial-state interaction (ISI), followed by two-nucleon absorption. In a similar fashion, following the two-nucleon absorption, one has the possibility that one or both of the energetic nucleons can undergo a collision with the residual nucleus. This process we refer to as a final-state interaction (FSI). Such FSI processes can be further divided into "soft" and "hard." The soft FSI is the interaction of two particles occurring when their vector momenta are nearly equal. Due to the fact that the nucleons from two-nucleon absorption in this experiment typically have momenta of 500 MeV/c, and the fact that the soft FSI populate such a small region of phase space, we expect the contributions from soft FSI's to our integrated yields to be negligible. Therefore, in the remainder of this paper we will use the term FSI to refer to hard collisions between the nucleons originating from absorption and the residual nucleus. For the proton energies relevant to this experiment, these processes correspond primarily to nucleon removal (p,pN) leading to at least four-body final states. Any realistic es-

[a]Present address: CEBAF, Newport News, VA 23606.
[b]Present address: NINDS-NIH, Bethesda, MD 20205.
[c]Present address: University of Liverpool, Liverpool, England.
[d]Present address: Arizona State University, Tempe, AZ 85287.
[e]Present address: IDA, Alexandria, VA 22311.
[f]Present address: New Mexico State University, Las Cruces, NM 88003.
[g]Present address: TRIUMF, Vancouver, B.C., Canada V6T 2A3.
[h]Present address: Physics Laboratory, State University of Utrecht, 3508 TA Utrecht, The Netherlands.
[i]Present address: Carnegie Mellon University, Pittsburgh, PA 15213.
[j]Present address: EMPA, CH-8600 Duebendorf, Switzerland.
[k]Present address: University of Geneva, Geneva, Switzerland.

timate of the total two-nucleon absorption cross section must include the effects of these ISI's and FSI's.

A number of groups have searched for direct experimental evidence of an ISI followed by two-nucleon absorption with apparently contradictory results. Some workers have sought and failed to find ISI-induced asymmetries in the angular correlation data on a variety of targets near the peak of the Δ resonance [6,7]. However, Brückner *et al.* [8] identified a peak in the forward angle proton energy spectra of their $^{12}C(\pi^+,3p)$ data for $T_\pi=240$, 260, and 289 MeV as being due to quasifree knockout. More recently, Tacik *et al.* [9] found less pronounced peaks at forward angles in their proton energy spectra on a ^{12}C target at 228 MeV. There have also been several reported observations [10,11] of the reaction (π^-,pp) with possible indications of ISI. Silk [12] has suggested that due to the short mean free path of the pion in the Δ-resonance region, it may be unreasonable to expect any experiment to kinematically distinguish between ISI-preceded two-nucleon absorption and multinucleon absorption.

Unequivocal experimental evidence for FSI is also minimal, although a 90° *p-p* correlation is indicated in the (π^-,pp) data of Yokota *et al.* [10]. In this case the relatively long mean free path of medium energy nucleons (~5 fm) [13] means that it is more reasonable to treat the absorption vertex and FSI as incoherent processes. This suggests that estimates of FSI contributions based on distorted waves or cascade calculations are more realistic than for the ISI.

A number of two-nucleon coincidence experiments have been performed near the Δ resonance [6,7,14]. In $(\pi^+,2p)$ measurements on nuclei ranging from ^{12}C to ^{209}Bi, at 165 and 245 MeV Altman *et al.* [7] find clear signatures of the two-nucleon mechanism. However, when these authors integrate those data which they believe arise from pure two-nucleon absorption, they obtain less than 10% of the total absorption cross section with a value of 9.2% for ^{16}O. Using internucleon cascade calculations to correct for the FSI, they estimate that less than 30% of the ^{16}O absorption cross section is due to two-nucleon absorption, thereby implying a dominance of multinucleon ($N>2$) absorption, in agreement with the conclusions of McKeown *et al.* [4]. However, in recent measurements also at $T_\pi=165$ MeV, Hyman *et al.* [15] obtain cross sections for ^{16}O, a factor of 2.3 larger than in the work of Altman. Using a distorted wave impulse analysis (DWIA) to estimate the FSI, they conclude that at 165 MeV, ~45% of the ^{16}O total reaction cross section is due to two-nucleon absorption.

For heavier nuclei Burger *et al.* [6] measured $^{58}Ni(\pi^+,2p)$ at 160 MeV. They estimate a pure two-nucleon absorption fraction of about 9% (approximately a factor of 2 larger than the Fe results of Altman *et al.*), which they correct for a FSI to ~32%. Thus, the experiments of Hyman *et al.* and Burger *et al.* would seem to indicate that near 165 MeV two-nucleon absorption yields are $\lesssim 50\%$ of the absorption cross section, and by implication, establish important contributions from either multinucleon ($N>2$) absorption processes or large ISI contributions. Concerning the latter, both Altman *et al.* and Burger *et al.* argue that the lack of a pronounced asymmetry in the angular correlation data indicates the ISI are small.

At lower energy, $^{16}O(\pi^+,2p)$ experiments have been performed with good energy resolution. At 116 MeV the data are satisfactorily described by normalized DWIA quasideuteron calculations with $L=0$ and 2 quasideuterons [16]. When extrapolated, assuming a $\pi^+d\rightarrow pp$ angular dependence, an assumption confirmed by the present experiment, Schumacher *et al.* [16], after correcting for FSI, find a rather larger two-nucleon absorption yield with approximately 50% of the absorption cross section in the first 20 MeV of excitation alone. These results are consistent with the 59.6 MeV results of Wharton *et al.* on ^{16}O [17].

In other measurements well below the Δ resonance, Yokota *et al.* [10] have made measurements of $^{6,7}Li(\pi^\pm,pN)$ at $T_\pi=70$ MeV. Unfortunately, due to the large uncertainty (±50%) in the absorption cross section on these nuclei below 100 MeV, little can be concluded about the relative importance of quasideuteron absorption.

Recently, experiments have been performed in an attempt to measure directly the multinucleon absorption component. In general these experiments have suffered greatly from the lack of coverage of phase space, thereby requiring extremely large extrapolations in order to extract a cross section. Definitive results await the new experiments being done with 4π detectors. However, the present experiments provide some interesting indications. Data for ^3He [18,19], for incident pion energies around the Δ resonance, contain large contributions from two-nucleon absorption which is reasonably consistent with expectations of a $^3S_1$ *n-p* pair spectroscopic parentage of 1.5. However, away from the quasifree two-body kinematics, the data are consistent with three-nucleon phase space. The total yield for this three-nucleon process is obtained by integrating the full phase space distribution normalized to the data. Although there exist some discrepancies in the two experiments, the integrated yield represents up to about 25% of the total absorption cross section for ^3He [5]. Furthermore, the data indicate that this fraction increases with increasing energy over the range studied.

Kinematically complete experiments of pion absorption in which three nucleons are detected in the final state have also been carried out over a very limited region of phase space on ^4He at 120 MeV [20] and on ^{12}C at 130, 180, and 228 MeV [9]. These data also suggest a moderately strong three-nucleon mechanism (perhaps as much as 20% of the total absorption cross section for ^{12}C at the highest energy), but rely on phase space to describe all dependences on kinematic variables in order to carry out the very large extrapolation necessary to obtain a cross section. Quantitative conclusions with direct measurements of multinucleon final states await experiments with a vast improvement in phase space coverage.

Theoretical studies of pion absorption have proceeded along several paths. The most extensive studies of two-nucleon absorption are those of Ohta, Thies, and Lee [21], Gouweloos and Thies [22] and Chant and Roos [23].

These works have emphasized various aspects including the π-NN vertex treatment and the treatment of distortion for the incoming pion and outgoing nucleons. The calculations have had limited success in describing the magnitude of the available cross section data.

Theoretical studies of the role of multinucleon absorption have also been carried out. Girija and Koltun [24] have attempted to attribute the inclusive results to a two-nucleon mechanism, with very strong ISI. However, Schiffer [25] has pointed out that such a model would have difficulty reproducing the measured $(\pi^+,p)/(\pi^-,p)$ ratios. Brown *et al.* [26] proposed a more exotic mechanism involving double Δ production, which yields four nucleons in the final state. However, it has been suggested that such a mechanism would contribute little near the energies of the Δ resonance, only becoming important at significantly higher incident energy [27].

In a different approach Masutani and Yazaki [28] used an optical model analysis to decompose the various contributions to the π-nucleus reaction cross section. They decomposed the absorption cross section into direct absorption from the elastic channel, and absorption following one or more quasifree scatterings. They estimate that the fraction of absorption not preceded by a quasifree scattering decreases from about 90% near 50 MeV to about 35% near 230 MeV. If this estimate is correct, it is surprising that little, if any, clean evidence for ISI has been seen in the experiments. Unfortunately, such a model makes no predictions which would help in kinematically isolating such processes.

Finally, the calculations of Oset, Futami, and Toki [29] find increasing contributions from three-nucleon processes with increasing pion energy, principally from sequential Δ production. They estimate that the two-nucleon cross section is about 100% of the total cross section at very low energy, decreasing to about 50% near the peak of the Δ resonance. The distinction of this proposed process (sequential Δ production) from ISI and the experimental signature of such processes remains to be determined.

In the present work we have carried out a kinematically well-defined study of the reaction $^{16}O(\pi^+,pp)^{14}N$. This experiment was performed with good missing-mass resolution and covers a large range of the phase space populated by two-nucleon absorption. The goals of this exclusive study were twofold: (1) to provide detailed information on the angular and energy distributions of the two protons, which will shed light on the dynamics of the process, and (2) by means of the extensive coverage of the phase space to obtain a total cross section for the two-nucleon absorption process which is as much as possible model independent. Simultaneously, high quality inclusive (π^+,p) measurements were taken. These data were taken for comparison with the coincidence data in order to establish experimentally the FSI corrections required to obtain a total two-nucleon absorption cross section.

In Sec. II we discuss the experiment and in Sec. III we present the measured cross sections for both the inclusive and exclusive reactions. Section IV contains the details of our analysis to extract the two-nucleon absorption cross section. Finally, the results are summarized in Sec. V.

II. THE EXPERIMENT

The experiment was performed in the πM1 channel [30] at the Paul Scherrer Institute. A layout of the experiment is shown in Fig. 1. The mean center-of-target pion kinetic energy during the experiment was 115 MeV. One of the emergent protons from the $^{16}O(\pi^+,2p)$ reaction was detected in the SUSI magnetic spectrometer [31] located at an angle θ_1. The second proton was detected in a large solid angle plastic scintillator array ($\Delta\Omega \simeq 600$ msr) centered at an angle θ_2. In the following text we will subscript all kinematic variables associated with the spectrometer with a "1" and those in the scintillator array with a "2". The scintillator array angle θ_2 is the angle of the second proton measured in the reaction plane defined by $\hat{\mathbf{n}}=\hat{\mathbf{p}}_\pi\times\hat{\mathbf{p}}_1$, where p_π and p_1 are the momenta of the beam and the proton detected by the spectrometer, respectively. The angle β_2 is the angle of noncoplanarity measured in a plane normal to the reaction plane, defined by $\hat{\mathbf{p}}_2\times\hat{\mathbf{n}}$, where $\hat{\mathbf{p}}_2$ is the momentum of the second proton.

The detector energy ranges in SUSI and the plastic scintillator array were approximately 48 to 220 MeV and 30 to 225 MeV, respectively. An overall excitation energy resolution of approximately 4 MeV was achieved. Data were taken for five values of θ_1 from 30° to 133°. One angle setting (θ_2) of the plastic array was close to the

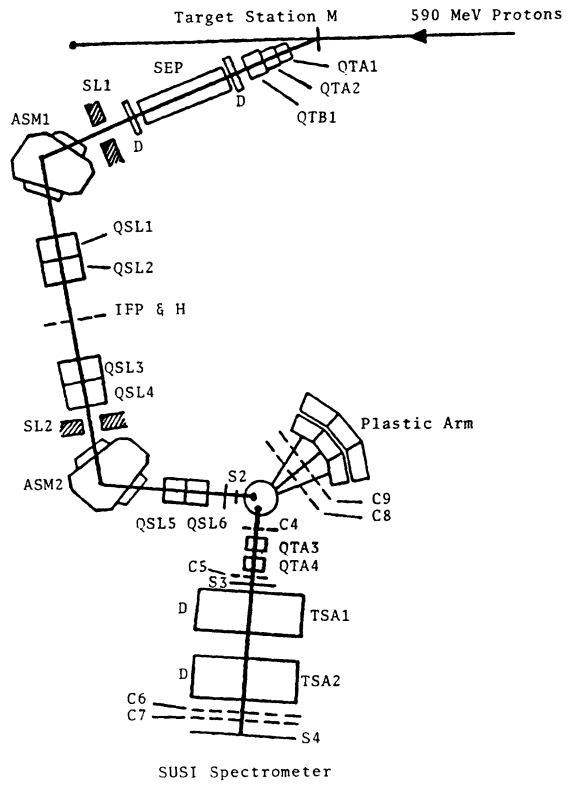

FIG. 1. The layout of the πM1 channel and the experimental hardware.

angle conjugate to θ_1 for protons from $\pi^+ d \rightarrow pp$ (quasifree angle pair). If beam and geometrical constraints permitted, two other settings of the plastic arm displaced $\pm 35°$ from the quasifree angle were made allowing measurements of the "wings" of the angular correlations. Because the horizontal acceptance $\Delta\theta_2$ of the detector was approximately 50°, there was always a significant overlap (typically one-third of $\Delta\theta_2$) between the quasifree and wing settings of the plastic scintillator array.

A. Apparatus

In the πM1 channel most protons were removed by an electrostatic separator. The pion beam ($\Delta p/p \simeq 4\%$) was dispersed at an intermediate focus onto a 16-element hodoscope. This hodoscope served to define the momentum of the incident pion to 0.25% (0.5 MeV) and to reject events with more than one pion within the rf microburst. Only about 50% of the events corresponded to a single pion in the hodoscope. The hodoscope efficiency after selecting single pion bursts was approximately 98%. To avoid biased sampling, the hodoscope efficiency was determined using random beam bursts.

Pions leaving the channel vacuum window passed through a 1 mm thick scintillator ($S2$) which was used to monitor the pion flux (4×10^6 π^+/sec) as well as to reject residual protons by pulse-height analysis, and muons and positrons by time of flight. Muons arising from pion decay following the final bend in the channel were $<10\%$ of the beam [30]. A good beam trigger was defined to be ($S2\cdot$rf) with pulse height and time-of-flight requirements satisfied.

At the target, the size of the beam spot was 1.0 cm vertical by 2.0 cm horizontal (FWHM). The target usually consisted of 4 mm of water (H_2O) sandwiched between 50 μm Mylar walls held by aluminum frames (20 cm wide $\times$10 cm high). A 2 mm thick target was used when energy losses of the two outgoing protons could not be well matched. An identical 4 mm D_2O target was used for absolute normalization. Frequent measurements of the targets showed that due to minute holes in the Mylar the thicknesses were shrinking at the rate of 0.1 mm per week. The thickness of the 4 mm D_2O target was linearly interpolated between measurements.

The SUSI magnetic spectrometer was used in a quadrupole-quadrupole-dipole-dipole configuration with a solid angle of approximately 13 msr. Pulse-height analysis was used on the spectrometer entrance scintillator $S3$ to reject most pion triggers. Because the minimum momentum accepted in SUSI was 300 MeV/c and the beam momentum was 213 MeV/c, it was not kinematically possible for pions to reach the exit scintillator $S4$ and generate a SUSI trigger (beam$\cdot S3\cdot S4$). Time-of-flight cuts were then used off-line to remove any surviving SUSI triggers not due to good protons ($\lesssim 0.2\%$). Multiple wire proportional chambers (MWPC's) with one x and one y plane each were placed in front of the first quadrupole and behind the second quadrupole, enabling both target spot reconstruction and more accurate recoil momentum determination. Near the focal plane of SUSI two x planes of MWPC's were used in the momentum determination of the protons. Altogether, six SUSI wire planes were used in the off-line analysis.

The large solid angle plastic scintillator detector consisted of three telescopes each employing a ΔE and two E detectors, which were 0.5, 15, and 15 cm in thickness, respectively. Each of the three telescopes was backed by a scintillator to flag events which did not stop in the E blocks. A plastic arm trigger (plastic) was defined to be (beam$\cdot$any ΔE). The solid angle of the three-telescope system was approximately 600 msr ($\Delta\theta_2 \simeq 48°$, $\Delta\beta_2 \simeq \pm 24°$). Light emitting diodes, pulsed once per second, were used to help correct short-term gain variations of the ΔE and E detectors off-line. The energy resolution was 3.5 MeV for 100 MeV protons. Two pairs of x-y MWPC's in front of the ΔE detectors enabled both a target spot reconstruction and improved angular resolution. The excellent energy resolution for such a large volume plastic scintillator was only possible because the wire chamber information allowed us to correct for attenuation of the light in the plastic. Finally the experimental coincidence event trigger was (SUSI$\cdot$plastic).

B. Corrections to data

The relative acceptance of the SUSI spectrometer over momentum was determined from inclusive (π^+,p) data by demanding consistency between the 4 and 5 overlapping momentum bites taken at each angle. A single acceptance function was used to simultaneously correct all five angle settings. Approximately 85% of all tracks lay within a smooth, easily corrected momentum acceptance of $\pm 12\%$. The acceptance correction was over a factor of 2 beyond these points; the remaining 15% of the tracks were excluded. Also rejected were events outside a peak in the angular correlation between the trajectory entering and leaving the spectrometer. This amounted to 1% of all SUSI events.

The largest correction, apart from the beam hodoscope losses, was due to wire chamber inefficiencies. Altogether ten wire planes were used, six in the SUSI spectrometer and four in the plastic arm. Combined inefficiencies were typically 37.5% due to a zero or multiple hits in any one of the wire planes. No significant energy and/or positional dependence of the chamber inefficiencies was found. We estimate the errors in a typical momentum sharing distribution, resulting from combining the errors in the focal plane acceptance correction, the error in momentum bin size, and chamber inefficiencies, to be $<5\%$.

Although use of the light-emitting diodes on the plastic scintillators to correct short-term gain variations improved the resolution slightly, there was a shift in gain from run to run which was typically less than 2%. This meant that, in general, the energy calibration for the plastic scintillators had to be redone for each run. As a guide to locate the expected centroid of the yield, the high resolution missing-mass spectra of Schumacher *et al.* [16] were used. That experiment was continuously calibrated via the reaction $\pi^+ d \rightarrow pp$.

Linearized ΔE vs E_{total} spectra were used for particle identification and for rejecting events due to nuclear reac-

tions in the plastic scintillator. While (π^+,pp) coincidences dominated, (π^+,pd) coincidences were observed to account for approximately 5% of the yield.

C. Normalization

The data were normalized to the published cross sections for $\pi^+d\rightarrow pp$ using the Legendre polynomial parametrization [32]. For a quasifree angle setting, protons from $\pi^+d\rightarrow pp$ provided coincidences between the magnetic spectrometer and the central telescope of the plastic array. In this configuration the SUSI spectrometer completely defined the solid angle. At each nonquasifree angle setting of the plastic arm, $\pi^+d\rightarrow pp$ normalization data were taken with a SUSI spectrometer trigger because the conjugate protons completely missed the plastic scintillator array. After corrections for nuclear reactions in the plastic scintillator [33], the normalizations obtained with coincidence and singles triggers were consistent to within $\pm 5\%$.

The uncertainty in the absolute normalization for both inclusive and coincidence data is due to errors in the measurement of the D_2O target thickness and in the determination of the ratio of the H_2O to D_2O target thicknesses via elastic scattering from ^{16}O. The absolute normalization for the inclusive data had an additional uncertainty resulting from the background beneath the $\pi^+d\rightarrow pp$ peak, while the coincidence normalization (which had negligible background) has an additional uncertainty due to the corrections for nuclear reactions in the plastic scintillator. Apart from statistical errors, the inclusive measurements are estimated to have overall uncertainties of $\leq 10\%$ and the coincidence measurements $\leq 12\%$. A more detailed description of the experimental apparatus and data analysis can be found in Ref. [34].

III. RESULTS

A. Inclusive $^{16}O(\pi^+,p)$ cross sections

In Fig. 2 are displayed inclusive $^{16}O(\pi^+,p)$ cross sections $d^2\sigma/d\Omega_1 dp_1$ for spectrometer angles θ_1 of 30°, 50°, 78°, 107.5°, and 133°. The displayed error bars represent counting statistics only. A broad peak is seen at each angle except 78°. This angle corresponds to 90° in the π^+d center-of-mass system where the $\pi^+d\rightarrow pp$ cross section is a minimum. The centroid of this peak agrees rather well with the momentum of protons from the reaction $\pi^+d\rightarrow pp$ corrected for the minimum Q value for removal of a deuteron from ^{16}O. To examine the quasideuteron aspects of the inclusive data somewhat further, in Fig. 2 the length of the vertical arrows represent the $\pi^+d\rightarrow pp$ cross section at each angle normalized at 30°. We see that the data are significantly above the arrows for the intermediate angles (78° and 107.5°). These observations are consistent with the inclusive data containing a strong quasideuteron component but with significant contributions from more complicated reaction mechanisms.

At 30° and 50°, the most forward angles, one sees evidence for a rise in cross section at the lowest momenta, the origin of which is probably the $^{16}O(\pi^+,\pi^+p)$ reaction. The energetic limit for (π^+,π^+p) scattering is marked in Fig. 2 at the forward angles by a short arrow on the momentum scale. Although it is energetically possible to have protons from the (π^+,π^+p) reaction underlying the 107.5° and 133° data, significant (π^+,π^+p) backgrounds near the peak are very improbable because the reaction would require a minimum nuclear recoil momentum of the order of 500 MeV/c. Other sources of background, which are presumably present at all angles, are multinucleon absorption mechanisms and initial- and final-state interactions accompanying the two-nucleon mechanism.

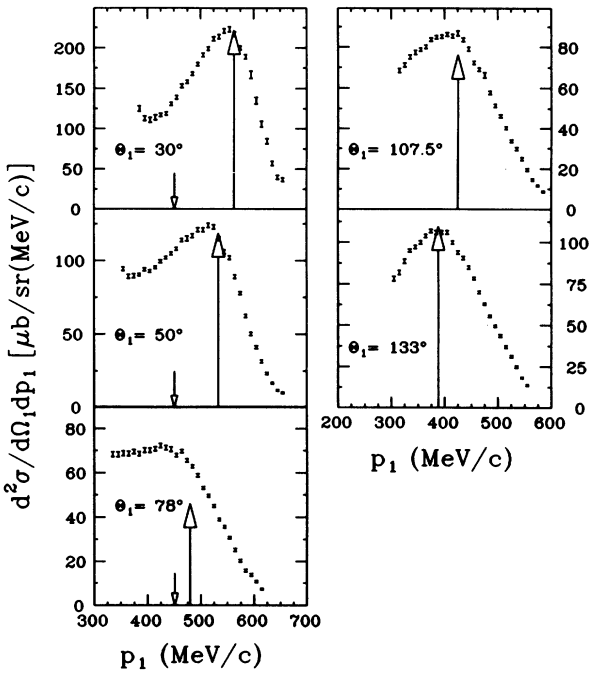

FIG. 2. The inclusive momentum spectra for $^{16}O(\pi^+,p)$ at 115 MeV. The long vertical upward arrow marks the momentum of a proton from the $\pi^+d\rightarrow pp$ reaction, corrected for one-half of the minimum deuteron binding energy in ^{16}O. The length of the arrow is proportional to the $\pi^+d\rightarrow pp$ laboratory cross section at 115 MeV, normalized at 30°. The short downward arrow at forward angles marks the kinematic endpoint for the $^{16}O(\pi^+,\pi^+p)$ reaction.

A survey of previous inclusive (π^+,p) data [4,35] suggests that while the two-nucleon absorption peak has long been observed for light targets at forward angles, it does not seem to be a generally recognized feature of the backward angle spectra. This is perhaps due to poor energy resolution near threshold in the previous studies. Note that the strong angular dependence of the two-nucleon absorption peak in these data precludes the use of a rapidity analysis as was performed by McKeown *et al.* [4]. It is clearly a poor approximation to assume that these protons arise from a thermalized source of N nucleons isotropically decaying in its rest frame.

B. Coincidence cross sections

In Fig. 3 we present typical excitation energy spectra of the residual nucleus ^{14}N for one spectrometer angle

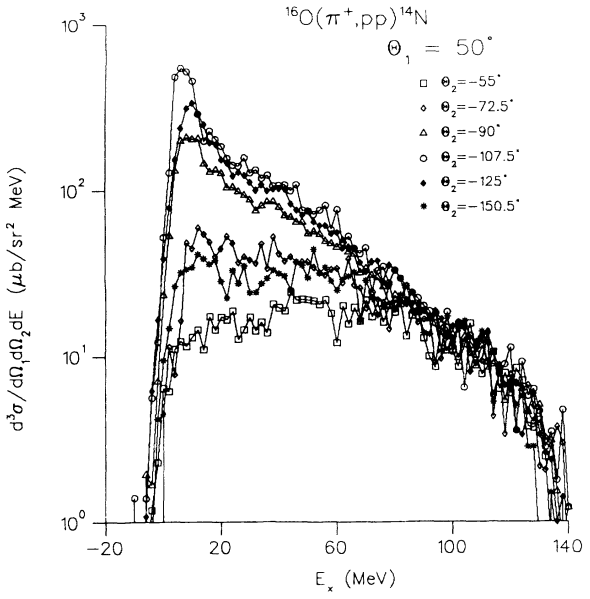

FIG. 3. Excitation energy spectra for the $^{16}O(\pi^+,2p)^{14}N$ reaction at 115 MeV. Each plot is for a proton angle of $\theta_1=50°$, the angle of the second proton being indicated on the figure.

$\theta_1=50°$ and various scintillator angles θ_2. Close to the quasifree angle of $\theta_2=-107.5°$ the excitation energy spectra are dominated by transitions to the 1^+ 3.95 MeV state, which is largely an $L=0$ transition [6,17]. Away from quasifree geometries an unresolved group of states dominated by $L=2$ transitions becomes more important, especially the 0, 7, and 11 MeV states of ^{14}N [16]. The cross section at low excitation is significantly larger for $\theta_2=-125°$ than at $\theta_2=-90°$. This asymmetry about the quasifree angle is due to the angle and energy dependence of the elementary $\pi^+(np)\rightarrow pp$ cross section [16,17]. Very far from quasifree angles (e.g., $-55°$, $-150.5°$), the missing-mass energy spectra are much smoother, showing little or no enhancement at low excitation energy. Above about 80 MeV excitation the yield shows little angular dependence.

1. *Momentum sharing distributions*

By restricting the excitation energy in the residual ^{14}N to be less than 20 MeV, we selected a data set which should be dominated by direct absorption (without ISI or FSI) on two p-shell nucleons. In Fig. 4 are shown the cross sections $d^2\sigma/d\Omega_1 dp_1$ for the quasifree angle setting. These data result from integration of $d^3\sigma/d\Omega_1 d\Omega_2 dp_1$ over the full solid angle of the plastic array ($\Delta\Omega_2 \simeq 600$ msr). An 8% correction to the data has been made for the yield that fell in the gaps between the ΔE counters, but there is no extrapolation beyond the physical extent of the detector.

The small arrow on the momentum axis marks the energy end point for coincident protons assuming a plastic arm energy threshold of 30 MeV and a transition to a level at 20 MeV excitation in ^{14}N. Thus, this arrow indicates the highest momentum for which the full excitation energy spectrum from 0 to 20 MeV is above the experimental threshold. The data above this end point are plotted as possibly useful lower limits.

In Fig. 4 we see that the data are characterized by a peak centered at an energy corresponding to $\pi^+d\rightarrow pp$ when corrected for Q value. The momentum distributions increase in width from forward to backward angles, which can be qualitatively understood in terms of the changing recoil momentum acceptance of the coincident large solid angle plastic detector. One also notes that the magnitude of the cross section at the peak is largest at $\theta_1=30°$, reaching a minimum at $\theta_1=78°$ and rising toward backward angles. This is reminiscent of the shape of the $\pi^+d\rightarrow pp$ angular distribution. Note that the distributions at $\theta_1=30°$, 50°, and 133° are asymmetric about the quasifree energy. A quantitative presentation of these effects will be given in Sec. IV A 1.

We now turn our attention to regions of excitation energy greater than 20 MeV. Although one expects considerable strength in this region due to absorption on s-p and s-s nucleon pairs, there are no narrow peaks observable in this region. Only a broad bump between 25 and 40 MeV is seen. This bump has also been observed by Schumacher *et al.* [16] in a better energy resolution measurement and by Hyman *et al.* [15] at 165 MeV. In those experi-

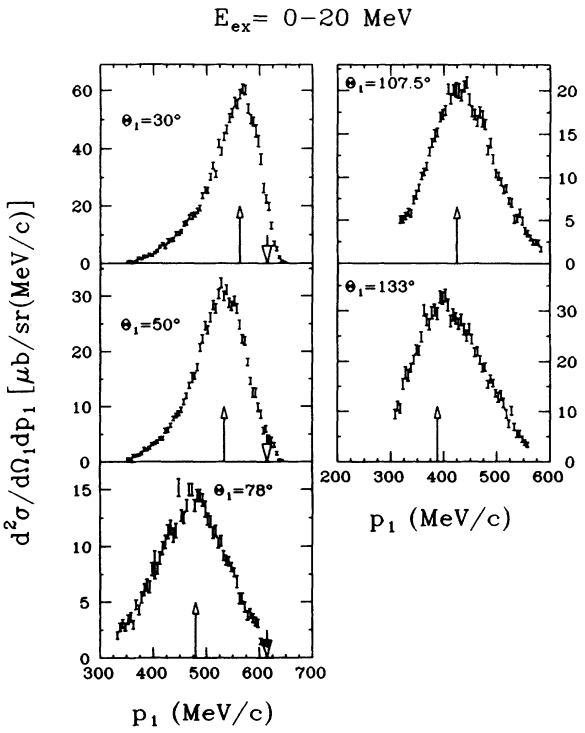

FIG. 4. Momentum sharing distributions for the $^{16}O(\pi^+,2p)^{14}N$ reaction at 115 MeV with 0–20 MeV of excitation energy in the residual nucleus ^{14}N. One proton was detected with the SUSI spectrometer set at θ_1. The coincident proton was detected with the large scintillator array ($\sim$600 msr) centered at the conjugate angle for the $\pi^+d\rightarrow pp$ reaction. The vertical arrow marks the momentum of a proton from $\pi^+d\rightarrow pp$ corrected for the deuteron binding energy in ^{16}O. The short downward arrows indicate the onset of the plastic scintillator threshold. Data above this point represent lower limits.

ments, as well as in this one, attempts to enhance the structure with restrictions placed solely on the magnitude of the recoil momentum were unsuccessful. However, DWIA calculations suggested that strong asymmetries are present in $L \neq 0$ angular correlations and momentum sharing distributions. (These asymmetries have been confirmed by Schumacher *et al.* [16].) In our DWIA model we expect absorption on *s-p* nucleon pairs to take place via an $L=1$ transfer to the residual nucleus. Therefore, in an attempt to enhance absorption on *s-p* pairs relative to all the background processes, we have used the predicted asymmetry and placed restrictions on the scintillator angle θ_2 and spectrometer momentum p_1, rather than the magnitude of the recoil momentum, to obtain the excitation energy spectrum shown in Fig. 5.

With this procedure we observe a statistically significant broad peak about 10 MeV wide and centered at 32±2 MeV of excitation. This peak was also observed at other angle settings. That this peak corresponds to absorption on a 1*s*-2*p* pair is suggested both by the high excitation energy (indicative of the participation of at least one 1*s*-shell nucleon) and by the fact that the transition is enhanced by placing restrictions on angle and momentum, which have been shown to preferentially select $L>0$ transitions. Of course, the DWIA calculations predict asymmetries for all $L>0$ transfers, so the $L=1$ nature (and thus the identification as *s-p* absorption) cannot be definitively established.

In Fig. 6 we display momentum sharing distributions for the 20–70 MeV excitation region which further demonstrate direct two-nucleon absorption strength at higher excitations. As before, the small downward arrow marks the point above which the data are affected by energy thresholds. The behavior of the peak magnitude is similar to that seen for 0–20 MeV of excitation, again consistent with the $\pi^+ d \rightarrow pp$ angular distribution. However, we find that the location of the centroid is now shifted relative to $\pi^+ d \rightarrow 2p$ indicated by the upward arrows. In Sec. IV A 1 we shall see that our DWIA calculations are able to account for this feature, providing more circumstantial evidence that this region is dominated by absorption on *s-p* pairs.

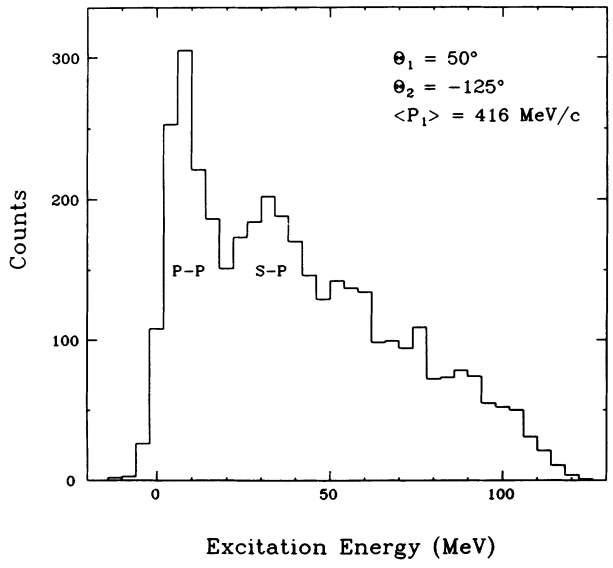

FIG. 5. Excitation energy spectrum for the $^{16}O(\pi^+,2p)^{14}N$ reaction. Selections in angle and momentum have been made to enhance the $L \neq 0$ two-nucleon absorption process ($\theta_1=50°$, $p_1=416\pm50$ MeV/*c*, $\theta_2=125°\pm7.5°$, $\beta_2=\pm23.8°$).

2. *Angular correlations*

As an alternative presentation of the data, we have generated angular correlations for the two excitation energy regions. In particular, for each spectrometer angle θ_1 we have integrated the triple differential cross sections $d^3\sigma/d\Omega_1 d\Omega_2 dp_1$ over the spectrometer momentum p_1. No extrapolation has been made into unmeasured regions of p_1. The resultant differential cross sections $d^2\sigma/d\Omega_1 d\Omega_2$ averaged over vertical strips (in-plane angle $\Delta\theta_2=\pm2°$ and noncoplanar angle $\Delta\beta_2=\pm23.8°$) in the plastic scintillator arm are presented in Figs. 7 and 8. Note that the averaging over our very large vertical acceptance results in significantly lower peak cross sections than would be seen in a small solid angle experiment.

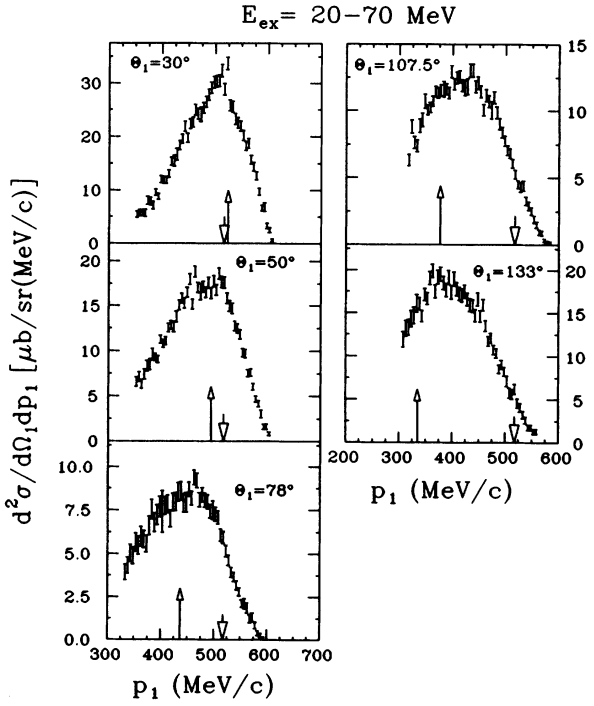

FIG. 6. Momentum sharing distributions for the $^{16}O(\pi^+,2p)^{14}N$ reaction at 115 MeV with 20 to 70 MeV of excitation energy in the residual nucleus ^{14}N. One proton was detected with the SUSI spectrometer set at θ_1. The coincident proton was detected with the large scintillator array (~600 msr) centered at the conjugate angle for the $\pi^+ d \rightarrow pp$ reaction. The vertical arrow marks the momentum of a proton from $\pi^+ d \rightarrow pp$ corrected for the deuteron binding energy in ^{16}O. The short downward arrows indicate the onset of the plastic scintillator threshold. Data above this point represent lower limits.

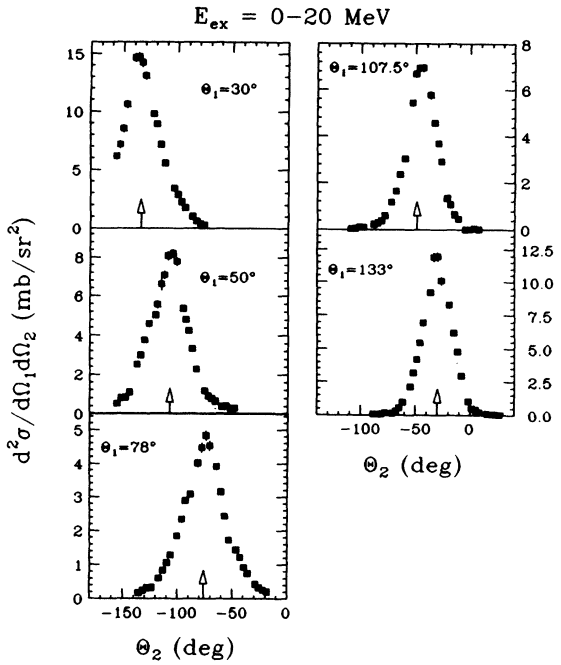

FIG. 7. Angular correlations for the $^{16}O(\pi^+,2p)^{14}N$ reaction at 115 MeV with 0 to 20 MeV of excitation energy in the residual nucleus ^{14}N. The cross sections are obtained by integrating over the momentum of the proton detected by the SUSI spectrometer ($\sim$300 to 600 MeV/c) set at θ_1. The cross sections are averaged over an angular range of the second proton of $\Delta\theta_2=\pm2.0°$ and $\Delta\beta_2=\pm23.8°$. The vertical arrow indicates the location of the $\pi^+d\rightarrow pp$ reaction corrected for the deuteron binding energy in ^{16}O.

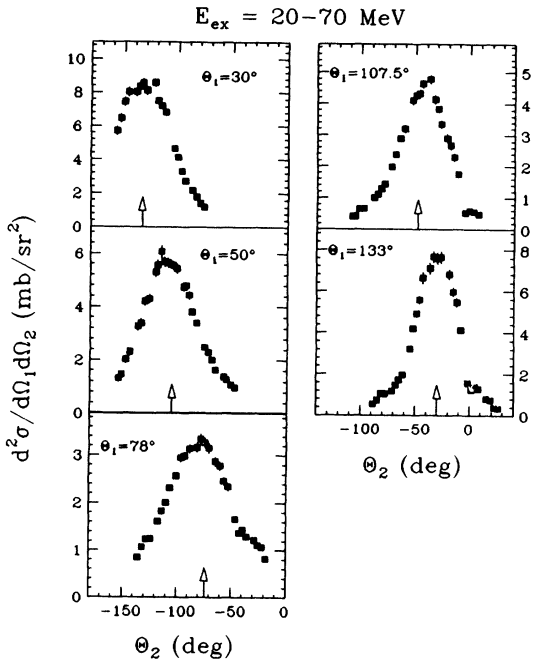

FIG. 8. Angular correlations for the $^{16}O(\pi^+,2p)^{14}N$ reaction at 115 MeV with 20 to 70 MeV of excitation energy in the residual nucleus ^{14}N. The cross sections are obtained by integrating over the momentum of the proton detected by the SUSI spectrometer ($\sim$300 to 600 MeV/c) set at θ_1. The cross sections are averaged over an angular range of the second proton of $\Delta\theta_2=\pm2.0°$ and $\Delta\beta_2=\pm23.8°$. The vertical arrow indicates the location of the $\pi^+d\rightarrow pp$ reaction corrected for the deuteron binding energy in ^{16}O.

Since the angular correlations are 40° to 50° wide, this reduction is of order a factor of 2.

For both excitation energy regions the angular correlations are strongly peaked near the conjugate angle for $\pi^+d\rightarrow pp$. The correlation is broader for the higher excitation energy region. Part of this arises naturally from the fact that the pion absorbs on the more tightly bound s-p pairs which have a broader momentum distribution. The remaining broadening presumably reflects the presence of more complicated reaction mechanisms.

IV. THEORETICAL ANALYSIS

We have compared the present experimental data with factorized DWIA calculations based on a quasideuteron absorption model. These comparisons play an essential role in helping to identify two-nucleon absorption strength in the continuum and in the extrapolation of the results to unmeasured regions of phase space.

Calculations of both exclusive $^{16}O(\pi^+,pp)$ and inclusive $^{16}O(\pi^+,p)$ were carried out using the distorted wave impulse approximation (DWIA). The theoretical formalism has been presented in detail by Chant and Roos [23]. Due to the large number of calculations required to compare with the experimental data, we have made two simplifying assumptions. First, we have omitted the spin-orbit potentials in the outgoing proton optical model potentials. This omission changes the calculations by less than 10% [23]. Second, we have factored out the two-body $\pi^+d\rightarrow pp$ cross section. As shown by Gouweloos and Thies [22] and by Chant and Roos [23], this procedure neglects tensor polarization effects of the deuteron cluster, effects which give rise to J dependence in the reaction. However, Chant and Roos [23] have shown that for closed-shell nuclei, data summed over all states of a given (j_1j_2) configuration will not exhibit J dependence. [This independence with J is modified slightly by a dependence of the reactions on Q value, but the effect is small ($\lesssim$15%)]. Thus, the factorized cross section treatment should be suitable for the present data, viz., we assume that ^{16}O is a closed shell and use the Cohen and Kurath [36] wave functions; the excitation energy cut of 0 to 20 MeV exhausts the bulk of the $(p)^2$ absorption strength; and the 20 to 70 MeV excitation energy cut contains the $(1s\,1p)$ absorption strength.

We, therefore, adopt the simple product approximation [23,27] (SPA), and the present calculations are essentially identical to those carried out for the high resolution $^{16}O(\pi^+,2p)^{14}N$ experiment of Schumacher *et al.* [16]. In particular, in the SPA the triple differential cross section for the $A(\pi^+,2p)B$ reaction to a specific final state in nucleus B with angular momentum L (z-projection Λ) can be written as

$$\frac{d^3\sigma}{d\Omega_1 d\Omega_2 dE_1}=\mathrm{KF}\frac{d\sigma}{d\Omega}\sum_{\Lambda}|T_{BA}^{L\Lambda}|^2 \qquad (1)$$

where KF is a known kinematical factor, and $d\sigma/d\Omega$ is taken to be the on-shell $\pi^+ d \rightarrow pp$ cross section [32]. The amplitude $T_{BA}^{L\Lambda}$ is given by

$$T_{BA}^{L\Lambda} = (2L+1)^{-1/2} \int \chi_{p_1}^{(-)*}(\mathbf{r}) \chi_{p_2}^{(-)*}(\mathbf{r}) \chi_{\pi}^{(+)} \times \left[\frac{B}{A} \mathbf{r} \right] \varphi_{L\Lambda}(\mathbf{r}) d^3 r \ , \quad (2)$$

where χ represents distorted waves. For these we have used the same optical model potentials as Schumacher *et al.*, i.e., the π^+-^{16}O optical model potential from Amman *et al.* [38] and the p-^{14}N potentials from Nadasen *et al.* [13].

The quantity $\varphi_{L\Lambda}$ in Eq. (2) is a microscopic form factor, as described in Refs. [16] and [23], representing the center-of-mass motion of the $^3S_1$ quasideuteron in the nucleus. For the low-lying positive parity states we have used the p-shell wave functions of Cohen and Kurath [36] to describe the states in ^{14}N. In this model only transitions to the $T=0$ 1^+(0, 3.95, 15 MeV), 2^+(7.03 MeV), and 3^+(11 MeV) states can occur. It is the sum of cross sections of these states for which the SPA is nearly identical to the more detailed calculations [23].

For absorption on $1s$-$1p$ pairs we have used the same microscopic quasideuteron model which only permits transitions to the following negative parity states: $(p_{1/2}^{-1} s_{1/2}^{-1})_{0^-,1^-}$ and $(p_{3/2}^{-1} s_{1/2}^{-1})_{1^-,2^-}$. Since these states are expected to be broad, we have assumed pure configurations and taken them to be degenerate at 32 MeV of excitation in ^{14}N, the location of the broad peak shown in Fig. 5. Again, the sum of cross sections will exhibit no J dependence. Finally, there is also a relatively small contribution from $(s_{1/2}^{-2})_{1^+}$ pairs, which we assumed to lie at an excitation energy of 45 MeV.

In spite of the various approximations and limitations of the quasideuteron DWIA model [23], the calculations describe the dependencies of the data on kinematic variables extremely well. This agreement indicates that much of the kinematic dependence of the two-nucleon absorption process is simply contained in the two-body $\pi^+ d \rightarrow pp$ cross section and the dependence of the amplitudes $T^{L\Lambda}$ on recoil momentum. The major discrepancy between the theory and experimental data lies in the necessity of applying a rather large renormalization factor (as much as a factor of 10) to the calculations to bring the two into agreement. Similar renormalizations are needed for the data of Ref. [16] for specific final states in ^{14}N. The origin of this discrepancy in magnitude may be due in part to nuclear structure, due to limitations in the shell model space, and/or due to the reaction dynamics, such as the inclusion of only absorption on $^3S_1$ pairs in the calculation. However, since the model adequately predicts the dependence on the kinematic variables such as angle and recoil momentum, we will use the calculations, renormalized to the data, to integrate into regions of phase space not measured in the present experiment.

A second crucial role for the DWIA in the analysis is to provide an estimate of the effect of final state interactions (FSI) between the residual nucleus and the outgoing protons. To make this estimate we have assumed that the final-state interactions, which remove yield from the direct two-nucleon absorption peak, are properly described by a complex proton optical model potential. Thus, we assume that a set of three (renormalized) DWIA calculations will provide us with the FSI correction, as well as a test of our treatment of the attenuation of the outgoing protons. These calculations are the following. (1) Calculations with the full proton optical model potential for both protons (σ_2) should describe the exclusive $(\pi^+,2p)$ two-nucleon absorption data. These calculations represent our directly observed two-nucleon absorption cross section. (2) Calculations with the imaginary part of the proton optical potential set to zero for the undetected proton (σ_1) should describe the two-nucleon absorption component of the inclusive (π^+,p) data. (3) Calculations with the imaginary parts of both proton potentials set to zero (σ_0) should describe two-nucleon absorption with no FSI. It is the ratio $(\sigma_0)/(\sigma_2)$ averaged over the proton energy acceptance which we take as our estimate of the effects of FSI. We then multiply the directly measured two-nucleon absorption cross section by this ratio to obtain the total two-nucleon absorption cross section.

The FSI correction factor is very large (~ 2.5) and thus has a major impact on our results for the total two-nucleon absorption strength. Assessment of the accuracy of the method is difficult. We first note that our calculations suggest that interference effects between the distorted waves are small, which is consistent with the observation that the distorted waves for the energetic protons behave essentially as attenuated plane waves. Thus, the predicted ratio σ_2/σ_0 is nearly equal to $(\sigma_1/\sigma_0)^2$ ($<4\%$ difference), and a 20% increase in the imaginary parts of the proton optical potential leads to an approximately 20% reduction in the cross section σ_2, in agreement with mean free path considerations.

Assuming the method to be correct, one can question the choice of proton optical model potentials. Those of Nadasen *et al.* [13] used in this analysis typically lead to a mean free path of the order of 5–6 fm, consistent with the theoretical work of Negele and Yazaki [39]. Recent works suggest the possibility of a somewhat shorter mean free path. For example, Dirac phenomenological analyses can often lead to a rather deeper imaginary potential. Also, a microscopic treatment of the propagation of nucleons in matter by Pandharipande and Pieper [40] would suggest a shorter mean free path, closer to 4–5 fm. The use of a shorter mean free path in our calculations of the FSI will clearly lead to an increased correction. For example, a reduction in the effective mean free path by about 1 fm leads to an increase in the FSI correction of about 20%, a result which was checked with DWIA calculations.

As experimental test of the method and choice of optical model potential, we point first to the work of Ref. [41]. Here the same type of calculations, using the potential of Nadasen *et al.*, are able to predict the ratio of $A(e,e'p)$ to $A(e,e')$ at the quasifree peak for a series of targets to better than 15%. This ratio represents the final-state interaction correction for the outgoing proton. (The average energy of the proton was 180 MeV in this

experiment.) There is an indication that for heavier nuclei the mean free path is somewhat shorter than that of the Nadasen *et al.* potential.

As a more direct experimental test for the case at hand, we have in the present experiment obtained inclusive $^{16}O(\pi^+,p)$ data. By isolating the two-nucleon absorption part of the inclusive cross section, we measure directly the ratio σ_1/σ_0 for comparison with the calculations. This ratio represents the correction for a FSI for a single proton. These results are presented and discussed in Sec. IV B and show the general accuracy of our method.

Finally, we note that in our present work we simply correct the total direct two-nucleon absorption cross section by the calculated FSI ratio without reference to angle or angular momentum. This procedure was checked by carrying out a series of DWIA calculations which showed that the variation in the FSI correction with angle was less than 2% over the range of the experiment and the variation with L was less than 10%. We have, however, taken account of the variation with excitation energy where the FSI correction increases by approximately 10% from the 0–20 MeV excitation energy region to the 20–70 MeV region.

The error in our FSI correction is difficult to estimate. However, all of the evidence discussed above suggests that if anything we have underpredicted the correction. Therefore, based on these considerations and our comparisons to experimental data as discussed, in the total cross sections we estimate an asymmetric error in our FSI corrections of roughly -10% and $+20\%$.

In the following sections we present the DWIA analysis of the data and the results for the total two-nucleon absorption cross section.

A. Coincidence results

1. Momentum sharing distributions

The curves in Fig. 9 represent $L=0$, $L=2$, and the incoherent sum of the $L=0+2$ transfers due to absorption on $(1p)^2$ pairs. The DWIA calculations have been integrated over the acceptance of the large solid angle plastic scintillator centered at the quasifree angle. To simplify the calculations, effects due to the finite solid angle of the SUSI spectrometer, the finite size of the beam spot, and the angular divergence of the pion beam were not included. These effects are small in comparison to the averaging created by the 600 msr solid angle of the plastic scintillator. A reasonably good overall fit to all angles was obtained by a single renormalization of the $L=0$ calculations by a factor of 10.0 and of the $L=2$ calculations by a factor of 6.0. The $L=0$ normalization was chosen by comparing the DWIA calculations to the data for a small solid angle cut (9°×9°) in the scintillator array centered at the quasifree angle for $\theta_1=133°$. For this case the $L=0$ contribution is dominant with the $L=2$ contribution being less than 10% at the peak. Once the $L=0$ normalization was determined, the $L=2$ normalization was chosen to provide an overall fit to the data at all angles over the full acceptance. We believe it is significant that the $L=0$ renormalization is larger than that for the $L=2$ calculations, an observation which is confirmed by the data and calculations of Schumacher *et al.* [16]. The result may be providing information concerning contributions from *n-p* pair configurations other than $^3S_1$ ($n=0$). Such terms are expected to contribute more to the $L=0$ transitions than to the $L=2$ transitions.

While the model describes the overall shapes and relative magnitudes of the momentum sharing distributions reasonably well (the agreement being poorer for the narrower, forward angle spectra), it is clear that differences exist in the detailed shape. For example, the data do not possess the shoulders contained in the sum of the $L=0$ and $L=2$ calculations. Although this might be remedied by changing the mix of $L=0$ and $L=2$ contributions, the $L=0$ normalization should be well determined by the small solid angle cuts discussed above.

Although the peak cross sections displayed in Fig. 9 vary by about a factor of 4 from $\theta_1=30°$ to 78°, the calculations reproduce the angular dependence quite well. To show this more quantitatively, we have integrated both the calculations and the data of Fig. 9 over the range of data not affected by the detector energy threshold and displayed the results in Fig. 10. Because the calculation was normalized to the data, in Fig. 10 we plot the integrated data with only relative errors of about 5%. The agreement between the data and the DWIA calculations is good. The angular dependence of the calculation is

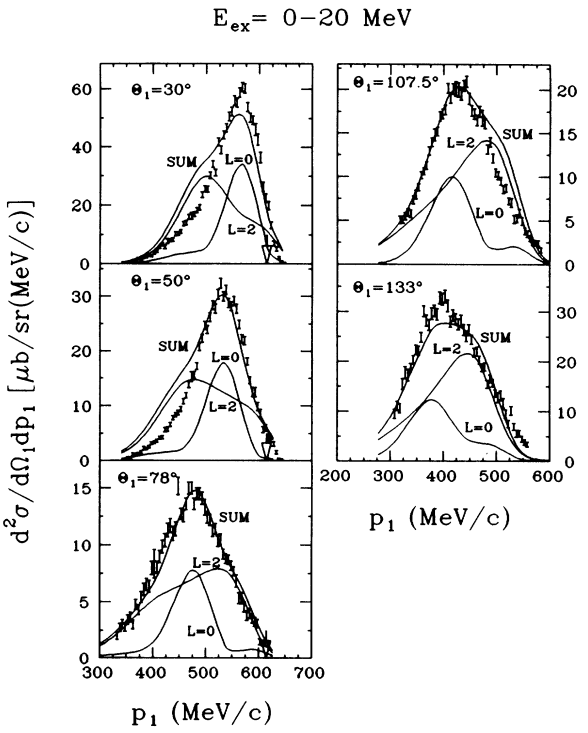

FIG. 9. Momentum sharing distributions for $^{16}O(\pi^+,2p)^{14}N$ at 115 MeV with 0 to 20 MeV of excitation energy (as in Fig. 4) compared to DWIA calculations of quasideuteron absorption on $(1p)^2\,^3S_1$ pairs. One $L=0$ and one $L=2$ normalization have been chosen as discussed in the text. The short downward arrows indicate the onset of the plastic scintillator threshold. Data above this point represent lower limits for the cross sections.

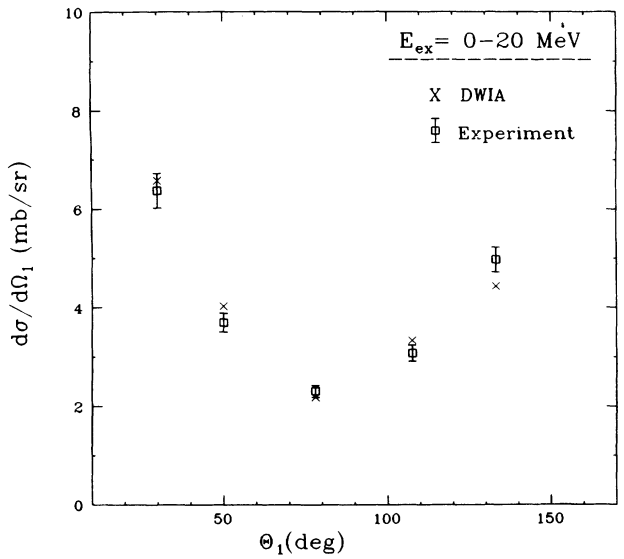

FIG. 10. Comparison of the cross sections integrated over momentum for the data and the DWIA calculations presented in Fig. 9.

dominated by the $\pi^+ d \rightarrow pp$ cross section. The differences between this angular distribution and that of $\pi^+ d \rightarrow pp$ is almost totally due to the acceptance of our experiment. For the first 20 MeV of excitation then, the two-nucleon absorption appears to be dominated by $\pi^+ d \rightarrow pp$ dynamics.

We turn now to the higher excitation energy region, 20–70 MeV. We have done calculations for absorption on $1s$ shell ($L=0$) pairs and ($1s$-$1p$) shell ($L=1$) pairs assuming the $(1p)^2$ contributions are negligible based on the shell model calculations. The $L=0$ strength is predicted to be small, and the renormalization was fixed at 10.0, the same as that determined for the $(1p)^2$ $L=0$ component. A restriction to a $\pm 5°$ region about the quasifree angle failed to show any peak in the momentum sharing distributions near the momentum expected for $L=0$ transfers, but did show significant asymmetry about the quasifree point as expected for $L \neq 0$ transfers. This could be due to there being three times as many $L=1$ pairs as $L=0$ pairs [21].

A renormalization of the $L=1$ calculations of 9.0 (in conjunction with the renormalized $L=0$ calculations) provided a reasonable fit to the peak cross sections for 50°–133°. The results are shown in Fig. 11. The 30° peak cross section is not reliable and represents a lower limit due to the energy threshold of the plastic arm. The calculation is narrower than the data at all angles, but approximately describes the magnitude near the peak.

These DWIA calculations provide a very natural explanation for the displacement of the centroid position from the corrected $\pi^+ d \rightarrow pp$ proton energy expectation previously seen in Fig. 6. These shifts arise from the asymmetries in the DWIA calculations due to the angle and momentum dependence of the two-body $\pi^+ d \rightarrow pp$ cross section. Although one suspects that there may be significant backgrounds due to more complicated processes such as multinucleon absorption or the FSI, two observations appear to be inconsistent with either or both of these processes dominating the 20–70 MeV of excitation region. First, the magnitude of the peak seems to be reasonably well described by quasideuteron DWIA calculations with a normalization factor comparable to the first 20 MeV of excitation. Second, the centroid is well predicted, which seems to require $L \neq 0$ transfers and dynamics similar to $\pi^+ d \rightarrow pp$. One would expect FSI contributions to be spread over a much larger region of angle and energy and, therefore, it would be surprising if the kinematic signatures of two-nucleon absorption remained so strong following the FSI. It appears then that the data between 20–70 MeV of excitation for quasifree angle pairs and our experimental acceptances are dominated by direct absorption on ($1s$-$1p$) pairs. It is impossible to be more quantitative within the context of our DWIA model. However, the more careful estimation of "backgrounds" in Sec. IV C yields nearly the same result.

2. *Angular correlations*

Although the primary comparisons of the DWIA calculations to the data were for the momentum sharing distributions, DWIA calculations were also carried out for the angular correlations for the 0–20 MeV excitation energy region. In this region, contributions from multinu-

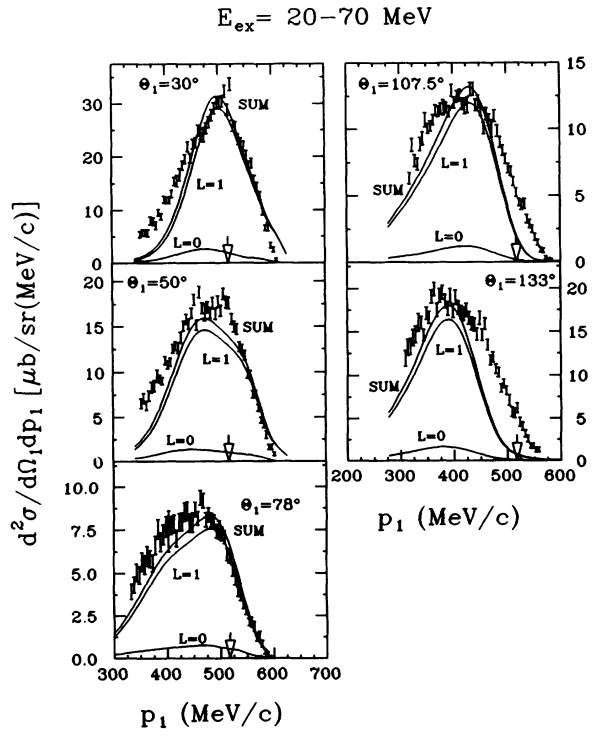

FIG. 11. Momentum sharing distributions for $^{16}O(\pi^+, 2p)^{14}N$ at 115 MeV with 20 to 70 MeV of excitation energy (as in Fig. 6) compared to DWIA calculations of quasideuteron absorption on ($1s$-$1p$) and $(1s)^2\,{}^3S_1$ pairs. One $L=0$ and one $L=1$ normalization have been chosen as discussed in the text. The short downward arrows indicate the onset of the plastic scintillator threshold. Data above this point represent lower limits for the cross sections.

cleon processes are expected to be very small so the comparisons are valid. The calculations, averaged over the experimental acceptance and normalized as in the preceding section, are shown in Fig. 12. The fits to the angular correlation data for 0 to 20 MeV excitation are quite good. The large asymmetry in the $L=2$ angular correlation, particularly for $\theta_1=50°$, is required by the data, as has already been emphasized in Ref. [16]. As before the angular dependence in the primary angle θ_1 is well reproduced by the DWIA calculations. It is clear that angular extrapolations of the data beyond the range of measurements using the DWIA introduce only small errors.

For the 20–70 MeV range of excitation, a comparison of the normalized DWIA calculation (normalized as in the preceding section) to the angular correlation data is not appropriate. These data contain significant multinucleon background as represented by the greater width of the momentum sharing data compared to the DWIA shown in Fig. 11.

B. Inclusive results

By turning off the imaginary part of the optical model potential for the undetected proton in the renormalized DWIA calculations and integrating over the entire angular correlation of the undetected proton, we are able to predict that part of the inclusive $^{16}O(\pi^+,p)$ cross sections, which is due to pion absorption on *n-p* pairs. Note that we introduce no new free parameters into the theory. Differences between the calculation and the data, beyond those noted in the comparisons to the exclusive data, are then presumed to be due to other processes such as FSI, ISI, or multinucleon absorption.

In Fig. 13 we see that the direct two-nucleon mechanism accounts for much of the angle integrated strength near the $\pi^+d\rightarrow pp$ proton energy. At 30°, where the two-nucleon absorption peak stands up most clearly in the data, the calculation implies little contribution from other processes. Contributions from (π^+,pn) [7] and (π^+,pd) [37], which contribute to the inclusive cross section, but are not included in the calculation, explain the approximate 10% difference between the calculation and the data at the peak. At 78°, however, where the peak disappears, the two-nucleon component is predicted to account for only about 65% of the strength near the $\pi^+d\rightarrow pp$ point. At backward angles, where the peak is again observed, a larger two-nucleon contribution is predicted. These comparisons suggest that the amount of two-nucleon strength predicted is approximately correct.

We note that phase space calculations suggest that at forward angles the two-nucleon component will be fairly well separated in momentum from any background that looks like three-nucleon phase space. This is not the case for backward angles. Furthermore, the rise in the $\pi^+d\rightarrow pp$ yield at forward lab angles also helps to increase the two-nucleon to background ratio. Therefore, we take the fact that our calculations essentially reproduce the peak of the data at 30° to mean that the attenuation of protons by the optical potentials used is satisfactory for this light nucleus and the proton energy range of this experiment. This comparison to the inclusive cross

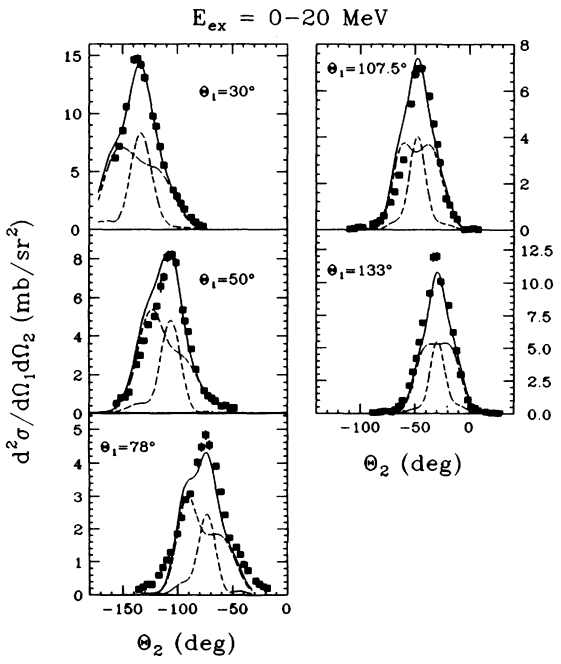

FIG. 12. Angular correlation for $^{16}O(\pi^+,2p)^{14}N$ at 115 MeV with 0 to 20 MeV excitation energy (as in Fig. 7) compared with DWIA calculations of quasideuteron absorption on $(1p)^2\,^3S_1$ nucleon pairs. The calculations include the experimental acceptance and are normalized as in Fig. 9.

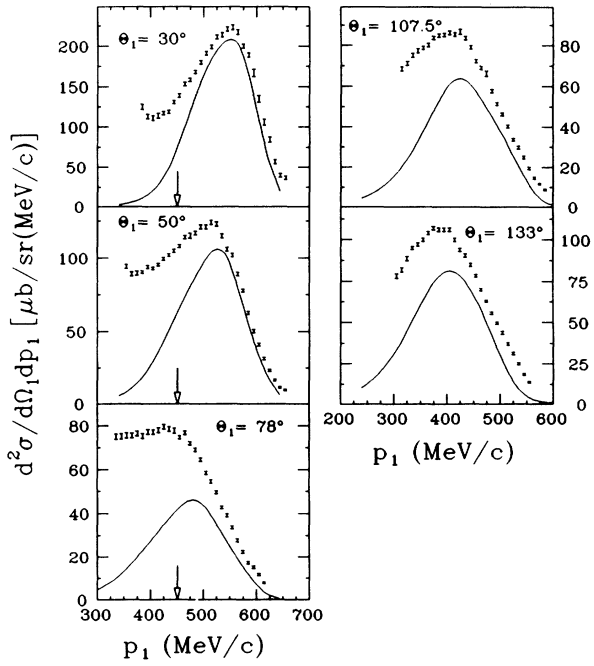

FIG. 13. Inclusive $^{16}O(\pi^+,p)$ cross sections (as in Fig. 2) compared with DWIA calculations (solid lines) of quasideuteron absorption on all $^3S_1$ nucleon pairs in ^{16}O. The DWIA calculations are normalized using the coincidence data as discussed in the text. The short downward arrow at forward angles marks the kinematic end point for the $^{16}O(\pi^+,\pi^+p)$ reaction.

section strongly supports our method and the magnitude of our FSI correction.

C. Estimate of the total quasideuteron absorption fraction

A primary goal of this absorption experiment was to determine the fraction of the absorption cross section due to a two-nucleon absorption mechanism. Above the particle breakup threshold of ^{14}N, four-body (or more) final states are populated. In this case it becomes increasingly difficult to separate two-nucleon absorption in which the resultant unstable nucleus decays by particle emission from other processes such as FSI, ISI, and multinucleon absorption in which the three nucleons are more directly involved in the reaction. This problem is exacerbated by the detection of only two of the protons. The extraction of the two-nucleon absorption strength is therefore model dependent. In the present experiment we have attempted to place severe restrictions on the data and the models by providing extensive coverage of the final states with good energy resolution. Therefore, extrapolations of the data to the unmeasured regions based on a model of the reaction are relatively small. Furthermore, corrections for FSI are checked by a comparison of the exclusive and inclusive data, so that again uncertainties should be small.

In the following we have chosen two methods of extracting the direct two-nucleon absorption contribution. In the first method the DWIA calculations, normalized to the momentum sharing distributions, were used both to extrapolate the results to the unmeasured regions and for the higher excitation energy region to separate the two-nucleon cross section from other processes. The second method does not rely on the DWIA calculations and is essentially the same method as that used in Refs. [6] and [7]. In this method fits to the angular correlations were used to make the extrapolation to the unmeasured angles, and the size of the background processes were determined from an analysis of the shape of the integrated differential cross section $d\sigma/d\Omega_1$. In both methods, after obtaining the direct two-nucleon absorption cross section, the DWIA results were used to correct for final-state interactions. Although the two methods are not totally independent, they are sufficiently different that we believe that a reasonably reliable fraction can be established.

1. DWIA based analysis

DWIA calculations were normalized to the momentum sharing distributions for 0–20 MeV of excitation as discussed in Sec. IV A 1. Once normalized, these calculations provide a good description of both the momentum sharing distributions and the angular correlations. When integrated the calculations yield 39±6 mb. This result confirms the angle extrapolated estimation of 38±5 mb by Schumacher *et al.* [16] for the same reaction and beam energy. Note that the DWIA serves essentially only to extrapolate the data to the unmeasured regions of phase space, since for the measured regions the integrated data and DWIA agree to better than 5% (see Fig. 10). These extrapolations contain 15–40 % of the cross section depending on angle, and we have taken an estimate of one-third of the value of the extrapolation as the error for each angle. A different mixture of the $L=0$ and $L=2$ contributions as discussed in Sec. IV A 1 has little effect on this integrated cross section. For example, an increase in the $L=0$ cross section by 15% with the appropriate reduction in $L=2$ to preserve the integrated yields in Fig. 10 only changes the total cross section by a few percent.

To proceed further one needs to subtract the FSI and multinucleon absorption backgrounds present in the data for the 0–20 MeV excitation region. We believe these backgrounds to be small, and for this analysis we ignore the contribution. Thus, in the first 20 MeV of excitation we find a cross section of 39±6 mb or approximately 19% of the total absorption cross section of 206±33 mb [42]. This number must then be corrected for losses due to the FSI which remove particles from the 0–20 MeV excitation energy range placing them at higher excitation energy. As discussed in detail above, we use DWIA calculations to predict a FSI correction factor of 2.5. Therefore, after corrections for the FSI, we find the cross section for two-nucleon absorption leading to the first 20 MeV of excitation in ^{14}N [due principally to $(1p)^2$ pairs] to be 98±15 mb, which represents 48% of the total absorption cross section. The error reflects the experimental uncertainty in the direct two-nucleon absorption cross section and does not include our estimate of the error in the FSI correction discussed before.

With 48% of the total absorption cross section corresponding largely to absorption on $(1p)^2$ pairs, a naive addition of the contribution from $(1s\text{-}1p)$ and $(1s)^2$ pairs would imply that the two-nucleon mechanism is dominant because slightly more than half of the $^3S_1$ pairs of nucleons in ^{16}O involve at least one nucleon in the s shell. This scaling by $^3S_1$ pairs probably overestimates the contribution of the inner shells, because the incident pion flux is attenuated in the interior. Furthermore, other NN configurations (e.g., configurations with nonzero oscillator quanta in the relative motion of the pair) almost certainly contribute to the 0–20 MeV excitation energy region, and these additional configurations constitute a smaller fraction for the inner shell pairs (due to the smaller number of available oscillator quanta).

We have already seen the qualitative evidence for significant direct two nucleon strength in the 20–70 MeV of excitation region. This took the form of a broad peak near 32 MeV of excitation and asymmetries in the momentum sharing distributions which were reproduced by our DWIA calculations. We saw, however, that the calculated distributions were narrower than the data.

Clearly, the extraction of the direct two nucleon contribution by integrating the DWIA distributions is suspect when there are significant differences between the data and the calculations. These differences presumably reflect contributions from more complicated processes such as multinucleon absorption and the FSI. Based on our analysis for the 0–20 MeV region, we expect a cross section of roughly 60 mb arising from the FSI following absorption on $(1p)^2$ pairs to be distributed into the higher

excitation energy regions. Our DWIA model provides no guidance concerning the distribution of these FSI events in phase space. In the unlikely event that these cross sections were all concentrated in the 20–70 MeV excitation energy range, but uniformly distributed in angle, we would expect constant contributions of less than about 1 μb/sr^2 MeV in the 20–70 MeV momentum sharing distributions. The DWIA to data comparison in Fig. 11 would certainly accommodate this level of background.

For now, in order to proceed we assume that the narrowness of the DWIA distributions will offset the presence of small backgrounds. We will return to the background question in the next section. We, therefore, integrate the DWIA calculations normalized as in Fig. 11. The result is 23±5 mb where the error includes an uncertainty of ±1 μb/sr^2 MeV for underlying backgrounds. This cross section is a little over 11% of the total absorption cross section. As anticipated, in spite of the fact that more $^3S_1$ pairs in ^{16}O are associated with at least one s-shell nucleon, we find the cross section to be only about 60% of that for the $(1p)^2$ configurations. Again, after correcting for losses due to FSI, we obtain a cross section of 64±14 mb for two-nucleon absorption on $(1s\text{-}1p)$ or $(1s)^2$ pairs or about 31% of the total absorption cross section. As before, this error does not reflect the uncertainty in the FSI correction.

Finally, this method of analysis using DWIA calculations indicates that about 79% of the absorption cross section is due to direct two-nucleon absorption. One expects there to be an additional small ($\lesssim$5%) contribution from $\pi^+ + (nn) \rightarrow p + n$ (Ref. [7]) which was not measured in this experiment.

2. *Angular distribution fit*

As an alternative method for extracting the two-nucleon absorption contribution, we have used fits to the angular correlation data to extrapolate to the unmeasured regions and have used phase space calculations to estimate the "background" in the integrated differential cross section $d\sigma/d\Omega_1$ due to more complicated processes. The angular correlations for different spectrometer angles (θ_1) shown in Figs. 7 and 8 were taken for two excitation energy regions of ^{14}N, 0–20 and 0–70 MeV, comparable to those regions used for the momentum sharing distributions. These correlations typically extend over a range of ±60° horizontal by ±25° vertical. A double-Gaussian fit to the more extensively measured horizontal correlation was used to extrapolate the data to an angular region of ±60° horizontal and ±60° vertical. The fits were used solely for extrapolation purposes without interpretation of their form. The vertical extrapolation increased the integrated cross section by about 25% for the 0–20 MeV excitation energy region and 40–50% for the 0–70 MeV region. For the most forward and backward θ_2 setting, the horizontal correlations were incomplete. In these cases a horizontal extrapolation of less than 10% was necessary. The extrapolated region of acceptance ($\sim\pm60°$) is expected to include all of the cross section for absorption leading directly to two-nucleon final states, plus a minimal "background" due to multiparticle final states. Integration of the fit to the angular correlations over this range of angle θ_2 for the two regions of excitation energy gave the differential cross sections $d\sigma/d\Omega_1$ shown in Fig. 14. No attempt was made to estimate the cross section missing due to the energy thresholds (see Figs. 4 and 6). The DWIA calculations (Figs. 9 and 11) indicate that this contribution is small.

The differential cross sections were fit by two components, the free $\pi^+ d \rightarrow pp$ cross section plus a normalized phase space distribution to represent background processes. The background was modeled by the quasifree process ^{16}O$(\pi^+, ppn)^{13}$N with a Gaussian spectator momentum distribution having a width $\sigma = 80\sqrt{3}$ MeV/c. A justification for this method comes from the work of Tacik *et al.* [9] who were able to describe extensive ^{12}C$(\pi^+, 3p)$ data. The restriction of our data to excitation energies less than 70 MeV should further suppress contributions from higher multiplicity final states. Background events within the region of extrapolation were generated using the Monte Carlo phase space code FOWL [43]. The angular distributions obtained did not depend strongly upon the excitation energy taken for the residual

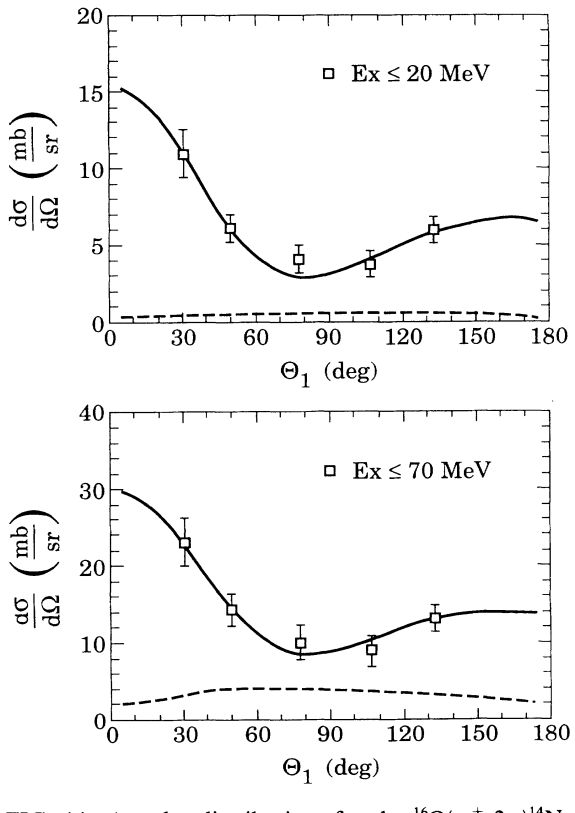

FIG. 14. Angular distributions for the ^{16}O$(\pi^+, 2p)^{14}$N reaction. (a) Data for 0 to 20 MeV excitation energy; (b) data for 0 to 70 MeV excitation energy. The dashed curves are normalized phase space calculations taken to represent the more complicated reaction processes. The solid curves represent the sum of the $\pi^+ + d \rightarrow pp$ differential cross sections [32] and the phase space calculations with normalizations chosen to best reproduce the experimental data. The relevant normalizations are indicated in the text.

TABLE I. Total two-nucleon absorption cross sections extracted from $^{16}O(\pi^+,2p)$ at 115 MeV.

Excitation	Total cross sections (mb)				Average cross sections with FSI	
	DWIA analysis		Two-Gaussian analysis			
energy	Unperturbed	Including FSI[a]	Unperturbed	Including FSI[a]	σ (mb)	σ/σ_{abs}(%)[b]
0–20	39±6	98±15	31±5	78±13	88±15	43%
20–70	23±5	64±14	27±4	74±11	69±14	33%
0–70	62±8	162±21	58±8	152±21	157±25	76%

[a]The error does not include any estimate of the uncertainty in the FSI correction. This is estimated to be roughly ±20% in the text.
[b]Assuming $\sigma_{abs}=206\pm33$ from Ref. [42].

^{13}N system. In fact, the following results would not be substantially different if an isotropic background were used.

The region of low excitation energy was expected to be relatively uncontaminated by continuum background, and the angular distribution closely follows the cross section for $\pi^+d\rightarrow pp$. The fits to the 0–20 MeV region shown in Fig. 14 used a $\pi^+d\rightarrow pp$ cross section normalized by 2.6±0.3 leading to an integrated cross section for the two-nucleon component $\sigma=31\pm5$ mb or about 15% of the total absorption cross section. The background cross section is 2.9 mb. Correcting for FSI losses as before increases the two-nucleon cross section to approximately 38% of the total absorption cross section, somewhat lower than the previous DWIA results. The difference arises partly from the assumption that some multinucleon absorption background underlies the 0–20 MeV two-nucleon absorption yield.

The full excitation region 0–70 MeV is expected to contain a more substantial background from multiparticle final states. In this case the fit yields a component which follows the $\pi^+d\rightarrow pp$ cross section with a normalization of 5.0±0.5 leading to a two-nucleon absorption component of 58±8 mb. The background cross section is 21.5 mb. Correcting for FSI leads to a two-nucleon absorption cross section of 152±21 mb or about 74% of the total absorption cross section, in good agreement with the DWIA analysis. Thus, both analyses imply the dominance of two-nucleon absorption at ^{16}O at 115 MeV.

The results of the two analyses for the extraction of the two-nucleon absorption cross section are summarized in Table I.

V. SUMMARY AND CONCLUSIONS

The two-nucleon absorption bump is a dominant feature of the inclusive $^{16}O(\pi^+,p)$ energy spectra at 115 MeV for both forward and backward angles. Only at 78° (which corresponds to the minimum of the $\pi^+d\rightarrow pp$ cross section) is the bump reduced to a shoulder. A rapidity analysis of these inclusive data is clearly inappropriate, being useful only when the decay of an N particle system is isotropic in its center of momentum. We have seen that the data in this region are in fact dominated by a strongly anisotropic $\pi^+d\rightarrow pp$-like cross section.

We have observed evidence not only for pion absorption on pairs of nucleons in the p shell, but also for the participation of at least one nucleon in the s shell. The data at high excitation are dominated by angular momentum $L>0$, which can be explained by absorption on $(1s$-$1p)$ pairs. No strong evidence for absorption on $(1s)^2$ pairs is seen in the 20–70 MeV of excitation region.

Direct two-nucleon absorption on n-p pairs uncorrected for FSI constitutes a total cross section of approximately 60±8 mb. Of this, about 60% comes from the first 20 MeV of excitation, corresponding mainly to absorption on $(1p)^2$ pairs. For the 0–20 MeV excitation energy region, extrapolation of the data to unmeasured regions of phase space was made using a DWIA model. For the 20–70 MeV region, corresponding primarily to absorption of $(1s$-$1p)$ pairs, two methods were used to extract the two-nucleon absorption cross section. One method relied on normalized DWIA calculations to identify and pick out the direct absorption strength in the data. The second relied on the assumption that the angular dependence of direct two-nucleon absorption is that of $\pi^+d\rightarrow pp$, while other processes produce the rather flat angular distributions expected for uniform population of phase space. Within errors both methods yield the same cross section.

Including corrections for losses due to FSI we conclude that direct two-nucleon absorption on n-p pairs leads to a total cross section of 157±25 mb. Although large corrections for the FSI were necessary, the fact that the calculations reproduce the ratio of the inclusive to exclusive peak cross sections at forward angles suggests that the magnitude of our corrections is good to better than 20%. Therefore, most of the uncertainty in the two-nucleon absorption cross section arises from our poor understanding of the backgrounds at high excitation due to other processes. Including estimates of the $\pi^+ + (nn)\rightarrow np$ channel and using the measured total absorption cross section of 206±33 mb, we conclude that approximately 80% of the total absorption cross section on ^{16}O at 115 MeV proceeds via two-nucleon absorption. This fraction excludes any contributions from the ISI which could lead to even larger percentages.

Therefore, we conclude that for this incident pion energy and target, the two-nucleon mechanism is dominant. Results for the reaction $^{16}O(\pi^+,pp)$ at 165 MeV [15] indicate that this two-nucleon absorption fraction of the total cross section decreases with increasing energy. Thus,

an overall picture of the pion absorption mechanism is emerging in which the two-nucleon mechanism is dominant for medium-light nuclei below the Δ resonance region.

Further advances in our understanding of the importance of the two-nucleon absorption mechanism will require improved experimental and theoretical treatment of the high excitation region where a significant fraction of the direct two-nucleon absorption cross section lies. The new generation of 4π detectors should help by allowing kinematically complete measurements of three- or more-nucleon final states, as well as providing essentially complete coverage of the two-nucleon absorption phase space.

ACKNOWLEDGMENTS

This work was funded in part by the National Science Foundation and the U.S. Department of Energy. The authors wish to express their gratitude to the staff at PSI who provided extensive support for this work.

[1] K. A. Brueckner, R. Serber, and K. M. Watson, Phys. Rev. **84**, 258 (1951).
[2] J. Favier, T. Bressani, G. Charpak, L. Massonnet, W. E. Meyerhof, and C. Zupancic, Nucl. Phys. **A169**, 540 (1971).
[3] E. D. Arthur, W. C. Lam, J. Amato, D. Axen, R. L. Burman, P. Fessenden, R. Macek, J. Oostens, W. Shlaer, S. Sobottka, M. Salomon, and W. Swenson, Phys. Rev. C **11**, 332 (1975).
[4] R. D. McKeown, S. J. Sanders, J. P. Schiffer, H. E. Jackson, M. Paul, J. R. Specht, E. J. Stephenson, R. P. Redwine, and R. E. Segel, Phys. Rev. Lett. **44**, 1033 (1980); Phys. Rev. C **24**, 211 (1981).
[5] H. J. Weyer, Phys. Rep. **195**, 295 (1990).
[6] W. J. Burger, E. Beise, S. Gilad, R. P. Redwine, P. G. Roos, N. S. Chant, H. Breuer, G. Ciangaru, J. D. Silk, G. S. Blanpied, B. M. Preedom, B. G. Ritchie, M. Blecher, K. Gotow, D. M. Lee, and H. Ziock, Phys. Rev. Lett. **57**, 58 (1986); Phys. Rev. C **41**, 2215 (1990).
[7] A. Altman, D. Ashery, E. Piasetzky, J. Lichtenstadt, A. I. Yavin, W. Bertl, L. Felawka, H. K. Walter, R. J. Powers, R. G. Winter, and J. v. d. Pluym, Phys. Rev. C **34**, 1757 (1986).
[8] W. Brückner, H. Döbbeling, P. C. Gugelot, F. Güttner, H. Kneis, S. Majewski, M. Nomachi, S. Paul, B. Povh, R. D. Ransome, T. A. Shibata, M. Treichel, Th. Walcher, P. Amaudruz, Th. Bauer, J. Domingo, R. Frey, Q. Ingram, H. Jantzen, G. Kyle, D. Renker, and R. A. Schumacher, Nucl. Phys. **A469**, 617 (1987).
[9] R. Tacik, E. T. Boschitz, W. Gyles, W. List, C. R. Otterman, M. Wessler, U. Wiedner, and R. R. Johnson, Phys. Rev. C **40**, 256 (1989).
[10] H. Yokota, K. Nakayama, K. Ichimaru, T. Katsumi, T. Mori, S. Igarashi, K. Hama, R. Chiba, K. Nakai, J. Chiba, H. En'yo, S. Sasaki, T. Nagae, and M. Sekimota, Phys. Rev. Lett. **57**, 807 (1986).
[11] Z. Papandreou, G. J. Lolos, G. M. Huber, J. C. Cormier, S. I. H. Naqvi, D. F. Ottewell, P. L. Walden, and G. Jones, Phys. Lett. B **227**, 25 (1989).
[12] J. D. Silk, Phys. Rev. C **37**, 891 (1988).
[13] A. Nadasen, P. Schwandt, P. P. Singh, W. W. Jacobs, A. D. Bacher, P. T. Debevec, M. D. Kaitchuck, and J. T. Meek, Phys. Rev. C **23**, 1023 (1981).
[14] A. Altman, E. Piasetzky, J. Lichtenstadt, A. I. Yavin, D. Ashery, R. J. Powers, W. Bertl, L. Felawka, H. K. Walter, R. G. Winter, and J. v. d. Pluym, Phys. Rev. Lett. **50**, 1187 (1983).
[15] S. D. Hyman, D. J. Mack, H. Breuer, N. S. Chant, F. Khazaie, B. G. Ritchie, P. G. Roos, J. D. Silk, P.-A. Amaudruz, T. S. Bauer, C. H. Q. Ingram, G. S. Kyle, D. Renker, R. A. Schumacher, U. Sennhauser, and W. J. Burger, Phys. Rev. C **41**, 409 (1990).
[16] R. A. Schumacher, P. A. Amaudruz, C. H. Q. Ingram, U. Sennhauser, H. Breuer, N. S. Chant, A. E. Feldman, B. S. Flanders, F. Khazaie, D. J. Mack, P. G. Roos, J. D. Silk, and G. S. Kyle, Phys. Rev. C **38**, 2205 (1988).
[17] W. R. Wharton, P. D. Barnes, B. Bassalleck, R. A. Eisenstein, G. Franklin, R. Grace, C. Maher, P. Pile, R. Rieder, J. Szymanski, and J. R. Comfort, Phys. Rev. C **31**, 526 (1985).
[18] K. A. Aniol, A. Altman, R. R. Johnson, H. W. Roser, R. Tacik, U. Wienands, D. Ashery, J. Alster, M. A. Moinester, E. Piasetzky, D. R. Gill, and J. Vincent, Phys. Rev. C **33**, 1714 (1986).
[19] G. Backenstoss, M. Izycki, P. Salvisberg, M. Steinacher, P. Weber, H. J. Weyer, S. Cierjacks, S. Ljungfelt, H. Ullrich, M. Furić, and T. Petković, Phys. Rev. Lett. **55**, 2782 (1985).
[20] G. Backenstoss, D. Brodbeck, M. Izycki, P. Salvisberg, M. Steinacher, P. Weber, H. J. Weyer, A. Hoffart, B. Rzehorz, H. Ullrich, D. Bosnar, M. Furić, and T. Petković, Phys. Rev. Lett. **61**, 923 (1988).
[21] K. Ohta, M. Thies, and T. H. S. Lee, Ann. Phys. (N.Y.) **163**, 420 (1985).
[22] M. Gouweloos and M. Thies, Phys. Rev. C **35**, 631 (1987).
[23] N. S. Chant and P. G. Roos, Phys. Rev. C **39**, 957 (1989).
[24] V. Girija and D. S. Koltun, Phys. Rev. Lett. **52**, 1397 (1984); **53**, 737 (1984).
[25] J. P. Schiffer, Phys. Rev. Lett. **53**, 736 (1984).
[26] G. E. Brown, H. Toki, W. Weise, and A. Wirzba, Phys. Lett. **118B**, 39 (1982).
[27] B. Schwesinger, A. Wirzba, and G. E. Brown, Phys. Lett. **132B**, 269 (1983).
[28] K. Masutani and K. Yazaki, Nucl. Phys. **A407**, 309 (1983).
[29] E. Oset, Y. Futami, and H. Toki, Nucl. Phys. **A448**, 597 (1986).
[30] J. P. Albanese, J. Arvieux, J. Bolger, E. Boschitz, C. H. Q. Ingram, J. Jansen, and J. Zichy, Nucl. Phys. **A350**, 301 (1980).
[31] *SIN User's Handbook* (SIN Laboratory Villigen, Switzerland, 1981), pp. 64–69.
[32] B. G. Ritchie, Phys. Rev. C **44**, 533 (1991).
[33] D. F. Measday, M. R. Menard, and J. E. Spuller, *TRIUMF Kinematic Handbook* (TRIUMF Laboratory, Vancouver, British Columbia, 1974), p. 3.2.
[34] D. J. Mack, Ph.D. thesis, University of Maryland, 1987.
[35] H. E. Jackson, S. L. Tabor, K. E. Rehm, J. P. Schiffer, R. E. Segel, L. L. Rutledge, Jr., and M. A. Yates, Phys. Rev. Lett. **39**, 1601 (1977); H. E. Jackson, S. B. Kaufman, L.

Meyer-Schützmeister, J. P. Schiffer, S. L. Tabor, S. E. Vigdor, J. N. Worthington, L. L. Rutledge, Jr., R. E. Segel, R. L. Burman, P. A. M. Gram, R. P. Redwine, and M. A. Yates, Phys. Rev. C **16**, 730 (1977).

[36] S. Cohen and D. Kurath, Nucl. Phys. **A141**, 145 (1970).

[37] P. G. Roos, L. Rees, and N. S. Chant, Phys. Rev. C **24**, 2647 (1981).

[38] J. F. Amman, P. D. Barnes, K. G. R. Doss, S. A. Dytman, R. A. Eisenstein, J. D. Sherman, and W. R. Wharton, Phys. Rev. C **23**, 1635 (1981).

[39] J. W. Negele and K. Yazaki, Phys. Rev. Lett. **47**, 71 (1981).

[40] V. R. Pandharipande and S. C. Pieper, Phys. Rev. C **45**, 791 (1992).

[41] D. F. Geesaman, R. Gilman, M. C. Green, R. J. Holt, J. P. Schiffer, B. Zeidman, G. Garino, M. Saber, R. E. Segel, E. J. Beise, G. W. Dodson, S. Hoibraten, L. D. Pham, R. P. Redwine, W. W. Sapp, C. F. Williamson, S. A. Wood, N. S. Chant, P. G. Roos, J. D. Silk, M. Deady, and X. K. Maruyama, Phys. Rev. Lett. **63**, 734 (1989); Phys. Rev. C **45**, 780 (1992).

[42] C. H. Q. Ingram, P. A. M. Gram, J. Jansen, R. E. Mischke, J. Zichy, J. Bolger, E. T. Boschitz, G. Pröbstle, and J. Arvieux, Phys. Rev. C **27**, 1578 (1983).

[43] F. James, CERN Computer Center Program Library, **W515** (1975).